Optics Letters

Monolithic integration of III-nitride voltage-controlled light emitters with dual-wavelength photodiodes by selective-area epitaxy

Chao Liu, Yuefei Cai, Huaxing Jiang, and Kei May Lau*

Department of Electronic and Computer Engineering, Hong Kong University of Science and Technology, Clear Water Bay, Kowloon, Hong Kong
**Corresponding author: eekmlau@ust.hk*

Received 17 April 2018; revised 31 May 2018; accepted 7 June 2018; posted 15 June 2018 (Doc. ID 328589); published 12 July 2018

We report for the first time on-chip integration of III-nitride voltage-controlled light emitters with visible and ultraviolet (UV) photodiodes (PDs). InGaN/GaN and AlGaN/GaN heterostructures were grown in specific regions by selective-area epitaxy, allowing monolithic integration of versatile devices including visible light emitting diodes (LEDs), visible-light PDs, AlGaN/GaN high electron mobility transistors (HEMTs), and UV-light Schottky barrier (SB) PDs. A serial connection between the LED and HEMT through the epitaxial layers enables a three-terminal voltage-controlled light emitter (HEMT-LED), efficiently converting voltage-controlled signals into visible-light signals that can be coupled into an adjacent visible-light PD generating electrical signals. While the integrated blue HEMT-LED and PD transmits signals carried by visible light, the visible-blind SB-PD on a chip receives external UV light control signals with negligible interference from the on-chip visible-light source. This integration scheme can be extended to open an avenue for developing a variety of applications, such as smart lighting, on-chip optical interconnect, optical wireless communication, and opto-isolators.

OCIS codes: (230.3670) Light-emitting diodes; (230.5170) Photodiodes; (040.7190) Ultraviolet; (130.3120) Integrated optics devices.

https://doi.org/10.1364/OL.43.003401

In analogy to their long-wavelength counterparts in silicon photonics, GaN-based building blockings for on-chip optical communications are being developed in recent years. Basic functionalities such as light generation, modulation, propagation, and detection can now be fulfilled with a suite of high-performance GaN-based components, including light emitting diodes (LEDs), high electron mobility transistors (HEMTs), waveguides, and photodiodes (PDs), making it possible to accomplish a sophisticated micro-opto-electronic system (MOES) on a chip by monolithic integration [1–3]. There has been much progress recently on monolithic integration of GaN-based devices, especially HEMT-LED integration [4–7]. Monolithically integrated HEMT-LED is a voltage-controlled light emitter, which is simpler to work with in driver design, compared to the conventional current-controlled LEDs. However, dramatic performance degradation was observed in the integrated devices reported initially, due to either material or process incompatibility [8,9]. Maintaining decent device performance after integration is of paramount importance. With a newly designed metal-interconnection-free lateral integration scheme [10] and a superior GaN/AlN buffer platform [11], we were able to demonstrate a voltage-controlled laterally integrated HEMT-LED with both the optical and electrical performance comparable to stand-alone devices [12].

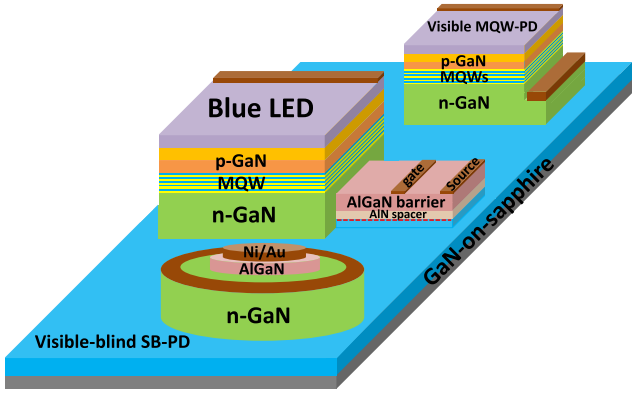

Fig. 1. Schematic illustration of a voltage-controlled HEMT-LED monolithically integrated with a visible MQW-PD (top) and a visible-blind Schottky barrier (SB)-PD (bottom).

To further explore the potential of monolithic III-nitride integration, we endow the existing HEMT-LED platform with additional functionalities. Under reverse bias, the quantum wells formed by InGaN/GaN and AlGaN/GaN heterostructures can efficiently capture visible and ultraviolet (UV) photons, create electron–hole pairs, and generate photocurrents. Figure 1 shows the schematic of the monolithically integrated MOES on a chip, which includes a blue voltage-controlled light emitter (HEMT-LED), a blue InGaN/GaN multi-quantum well (MQW) PD, and a UV AlGaN/GaN Schottky barrier

(SB) PD. The voltage-controlled HEMT-LED emits modulated visible light controlled by gate and drain biases of the integrated HEMT [10,12]. The visible InGaN/GaN MQW-PD exhibits synchronous photocurrents with the modulated light from the integrated HEMT-LED, which can be used as an electrical feedback signal. Meanwhile, the AlGaN/GaN SB-PD can receive an external UV light control signal without interference from the blue light emitted by the adjacent HEMT-LED. This monolithic integration scheme not only leverages the superior performance of GaN-based devices but also provides the best route towards a MOES with a reduced footprint, lower parasitics, and simplified packaging complexity.

The initial platform for integration was an AlGaN/GaN HEMT epitaxial structure grown on 2 in. sapphire substrates in an Aixtron 2400HT metal organic chemical vapor deposition (MOCVD) system. From bottom to top, the AlGaN/GaN HEMT structure included a 150 nm AlN nucleation layer, a 3 μm GaN buffer layer, a 100 nm GaN channel layer, a 1 nm AlN spacer layer, and a 20 nm $Al_{0.3}Ga_{0.7}N$ barrier layer [11,12]. Afterwards, a 200 nm SiO_2 layer was deposited by plasma-enhanced chemical vapor deposition (PECVD) and patterned by photolithography and buffered oxide etch (BOE). Inductively coupled plasma (ICP) etching was performed to selectively remove the AlGaN/AlN/GaN stack to expose the GaN buffer and the sidewall GaN channel of the AlGaN/GaN HEMT. Afterwards, selective epitaxial growth (SEG) of a standard LED structure was carried out on the etched region. The overgrown LED epi started with a 1.2 μm *n*-type GaN, serving as the cathode of the LED and the drain of the HEMT. Subsequently, three periods of InGaN/GaN shallow wells and five periods of InGaN/GaN MQWs were grown, followed by five periods of a *p*-type AlGaN/InGaN superlattice electron blocking layer, a 150 nm *p*-type GaN, and a 20 nm *p*-type InGaN contact layer.

Device fabrication started with the definition of mesas for the InGaN/GaN MQW LEDs and PDs by ICP etching, while the AlGaN/GaN HEMT and SB-PD region was protected by photoresist. Then, mesas of HEMTs and SB-PDs were created with the LED and PD area protected. Source ohmic contacts of the HEMTs and SB-PDs were formed by *e*-beam evaporation of Ti/Al/Ni/Au and rapid thermal annealing (RTA) at 850°C for 30 s in N_2 ambient. Afterwards, a Ni/Au current spreading layer and a Ti/Al/Ti/Au *p* electrode of the InGaN/GaN MQW LEDs and PDs were evaporated. Finally, Ni/Au gate metallization was realized for the HEMTs and SB-PDs. During SEG of the LED structure, an intimate interconnect between the *n*-type GaN cathode of the LED and the sidewall channel of the HEMT was formed [10]. Thus, the source pad of the HEMT and the *n* electrode of the LED were eliminated, and no extra metal wire was needed to connect the LED and the driving HEMT. Figure 2(a) presents a top–down view scanning electron microscope (SEM) image of the monolithically integrated HEMT-LED and dual-wavelength PDs. A circular layout was implemented in this experiment in an attempt to improve the current spreading capability from the integrated HEMT to the LED. Figure 2(b) shows the on-testing of the three-terminal HEMT-LED emitting divergent visible light, which propagates across the whole die and couples into the visible InGaN/GaN MQW-PD and the UV AlGaN/GaN SB-PD.

On-wafer characterization of the integrated HEMT-LED denotes effective control of the output current by the gate and drain biases of the integrated HEMT, as shown in Fig. 3. A driving current of 200 mA can be provided by the integrated circular transistor, corresponding to a current density of around 70 A/cm^2 for the integrated circular LED with a diameter of 600 μm. Other than a turn-on voltage of around 3 V induced by the LED connected in-series, the integrated HEMT-LED exhibits output characteristics similar to a discrete HEMT simultaneously fabricated on the same wafer. The optical output characteristics (L-V) of the HEMT-LED are determined by the drain current through the HEMT-LED. The value obtained is similar to its electrical I-V characteristics. The gradual droop in the I_{ds} of the HEMT and, thus, in the output of the LED beyond saturation is attributed to the self-heating effect in the direct current (dc) measurement, which results in thermally induced mobility degradation [13].

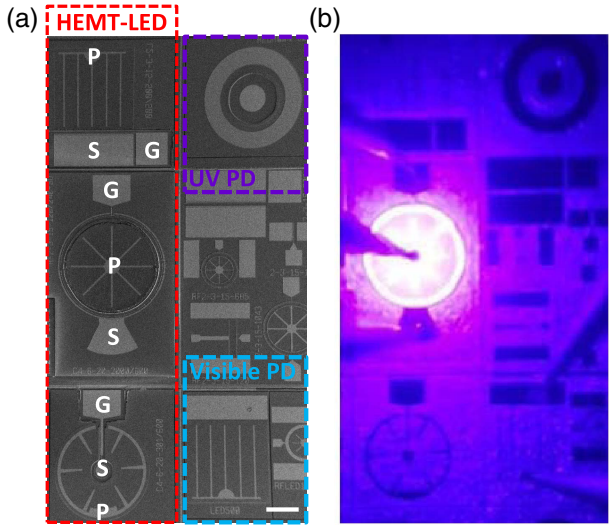

Fig. 2. (a) Top view SEM image of the HEMT-LED monolithically integrated with a UV PD and a visible PD, scale bar is 200 μm, and (b) on-testing HEMT-LED emits visible light, which propagates across the whole die and is received by the visible InGaN/GaN MQW-PD and UV AlGaN/GaN SB-PD.

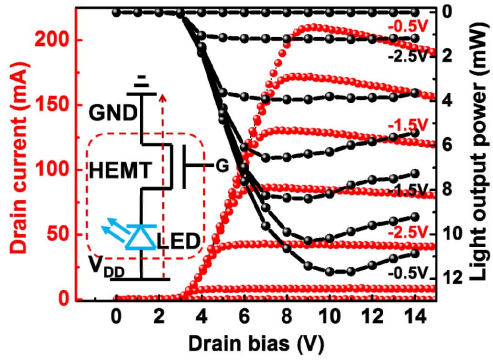

Fig. 3. Red curve, output characteristics (I-V) of the monolithically integrated circular HEMT-LED, $W_G/L_G = 2000$ μm/4 μm, $L_{GS}/L_{GD} = 6$ μm/20 μm, LED diameter = 600 μm; black curve, light output power of the circular HEMT-LED modulated by V_G and V_{DD}, $V_G = -0.5 \sim -4$ V with a step of −0.5 V; the inset is the equivalent circuit of the HEMT-LED.

With an electrical control signal upon the gate or drain terminal of the HEMT, the integrated LED can emit visible light with modulated intensity and duty cycle, which can serve as a downlink signal in a wireless optical communication system.

While a visible-light signal is generated from the voltage-controlled light emitter and propagating into free space, part of the divergent/scattered blue light can be received by the adjacent visible-light MQW-PD and converted into photocurrent signals, which can be utilized as an electrical feedback signal to monitor the working status of the HEMT-LED transmitter. The photocurrent signals are thus synchronized with the input control signals of the HEMT-LED transmitter. A dark current of 150 $\mu A/cm^2$ at a reverse bias of −5 V in Fig. 4(a) indicates decent performance of the integrated InGaN/GaN MQW-PD. With an increased gate bias of the HEMT-LED from −5 to 1 V at a drain bias of 5 V (linear region), the light output from the integrated HEMT-LED was gradually enhanced and received by the adjacent MQW-PD, resulting in a boosted photocurrent level. In addition to the gate modulation, the integrated HEMT-LED can also convert drain bias signals into modulated light emission. I-V characteristics of the modulated HEMT-LED-PD exhibit excellent responsivity of the integrated MQW-PD to the light signal from the HEMT-LED transmitter, controlled by the gate/drain bias voltages in Fig. 4(b).

The schematic energy band diagrams for the InGaN/GaN MQW-PD, InGaN/GaN MQW-LED, and AlGaN/GaN SB-PD are plotted in Fig. 5(a). Under positive voltage bias ($V > 0$), electrons and holes are injected into InGaN/GaN MQWs and recombined, generating visible light with photon energy of around 2.9 eV. The InGaN/GaN MQW-PD with a similar bandgap absorbs the 2.9 eV photons and generates electron–hole pairs, which are separated promptly by the strong local electric field under reverse bias. The AlGaN/GaN SB-PD, on the other hand, has a larger bandgap of around 3.4 eV and is transparent to the visible light with lower photon energy. To verify the functionality of the AlGaN/GaN SB-PD, reverse I-V curves of the SB-PD under different radiation sources [Fig. 5(b)] are plotted in Fig. 5(c). Under the halogen source with a peak wavelength of 650 nm, no photocurrent was observed, and a minor increase in the reverse current can be detected under the blue light from the integrated HEMT-LED. Under a UV light source with a wavelength of 365 nm, a dramatic increase in the reverse current density occurred, indicating an effective response of the UV SB-PD to the UV light. The minor response of the UV SB-PD to the blue light might be due to the intra-band absorption in the AlGaN/GaN triangular wells of the UV SB-PD. Further optimization of the epitaxial structure for the UV PDs and the blue LEDs should be carried out to eliminate the interference from the blue light to the UV PDs completely.

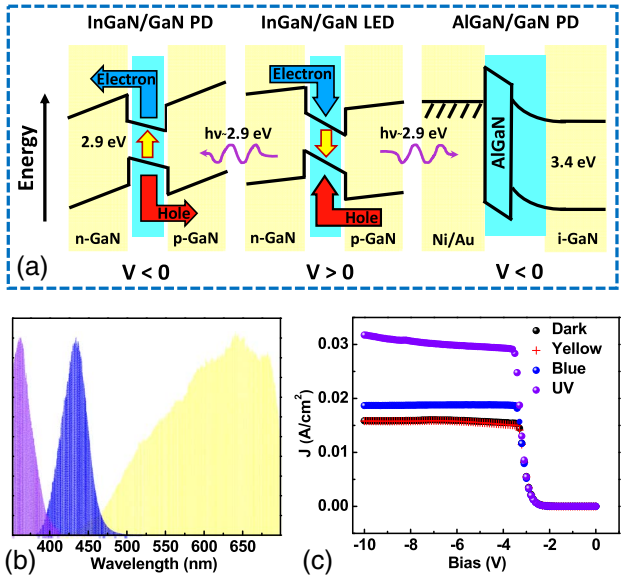

Fig. 5. (a) Schematic energy band diagrams for InGaN/GaN MQW-PDs, InGaN/GaN MQW LEDs, and AlGaN/GaN SB-PDs with negative ($V < 0$), positive ($V > 0$), and negative ($V < 0$) external voltage biases; (b) spectra of the external halogen light (yellow), UV light (violet), and blue light from adjacent HEMT-LED (blue); (c) dark current and photocurrent of the AlGaN/GaN SB-PD against reverse voltage biases under the illumination of different light sources.

A switching test was performed for the integrated MOES. An external resistor (1 MΩ) was connected in-series with the reversely biased (−5 V) visible PD to convert the photocurrent signal into a voltage signal that can be measured by an oscilloscope. A pulse voltage (0 ∼ −4.7 V) was applied on the gate terminal, and a control voltage of 6 V was applied on the p electrode of the integrated HEMT-LED to assure that the voltage-controlled light emitter switches within its linear region. Figure 6 illustrates the voltage-time curves of the gate bias and the measured bias at the n node of the visible PD.

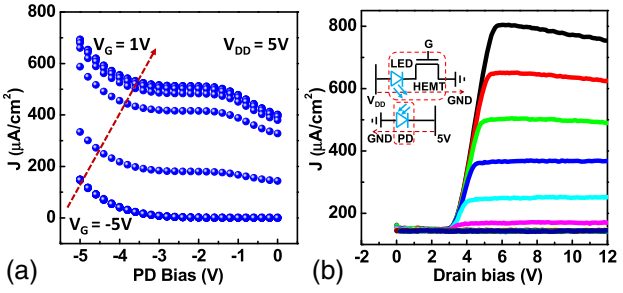

Fig. 4. Photocurrent of the InGaN/GaN MQW-PD: (a) against reverse bias of the PD at varied V_G biases of the integrated HEMT; (b) modulated by V_G and V_{DD} of the HEMT-LED; $V_G = -2.4$ to −6 V with a step of −0.2 V.

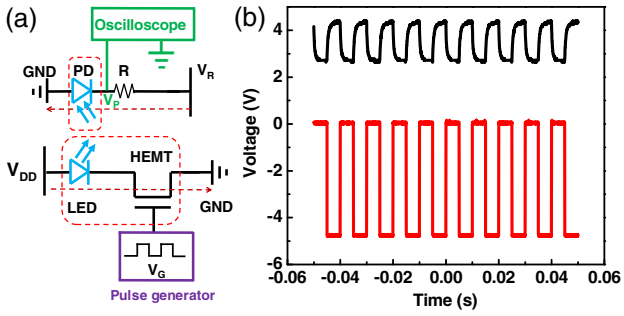

Fig. 6. (a) Equivalent circuit of the setup for the switching test of the HEMT-LED-PD MOES; (b) red curve, pulsed gate voltage signal; black curve, induced photocurrent temporal traces of the visible MQW-PD.

A synchronous rectangular waveform can be detected at a switching frequency of 100 Hz. Further increasing the pulse frequency will result in a triangular waveform output. This first demonstration can be used for smart outdoor lighting systems, in which the frequency is typically 50 or 60 Hz. It is noteworthy that the integrated HEMT-LED alone can work at a switching frequency up to 15 MHz, which showed great advantages as compared to Si-based MOES systems [14]. We suspect the switching speed of the HEMT-LED-PD system is in part limited by the large capacitance of the 500 μm × 500 μm visible PD and in part restricted by the external resistor (1 MΩ) in-series with the reversely biased PD. Further enhanced switching speed of the HEMT-LED-PD system can be achieved with an optimized test circuit and layout design so that the integrated system could be used for broader ranges of applications, such as opto-isolators, on-chip optical interconnects, and visible-light communications.

In conclusion, we demonstrate a micro-electro-optical transceiver system by monolithically integrating a III-nitride HEMT-LED with blue and UV PDs on a single chip. The three-terminal HEMT-LED is a voltage-controlled device that can deliver a visible-light signal controlled by the voltage signal on the gate and drain terminal of the HEMT. Part of the visible light is coupled into the blue PD and converted into an electrical signal, which can serve as an *in-situ* feedback signal. Meanwhile, the UV PD can receive an external UV light control signal with negligible interference from the downlink visible light. This monolithic solution marks a major step towards a number of applications, including smart lighting and wireless visible-light communication by photonic–electronic integration.

Funding. Research Grant Council of Hong Kong (16204714, T23-612/12-R).

Acknowledgment. We gratefully thank Qiang Li, Yu Han, Bei Shi, Yating Wan, Yuying Chen, Xianbo Li, and Jun Ma for fruitful discussions, and Wilson Tang as well as the staff of the MCPF and NFF of HKUST for their technical support.

REFERENCES

1. W. Cai, Y. Wang, X. Gao, J. Yuan, W. Yuan, H. Zhu, and Y. Wang, Opt. Express **24**, 6004 (2016).
2. Y. Wang, G. Zhu, W. Cai, X. Gao, Y. Yang, J. Yuan, Z. Shi, and H. Zhu, Appl. Phys. Lett. **108**, 162102 (2016).
3. Z. Jiang, M. R. M. Atala, G. You, L. Wang, X. Li, J. Liu, A. M. Elahi, and J. Xu, Opt. Lett. **39**, 5657 (2014).
4. F. G. Kalaitzakis, E. Iliopoulos, G. Konstantinidis, and N. T. Pelekanos, Microelectron. Eng. **90**, 33 (2012).
5. Z. Li, J. Waldron, T. Detchprohm, C. Wetzel, R. F. Karlicek, Jr., and T. P. Chow, Appl. Phys. Lett. **102**, 192107 (2013).
6. Y. Lee, Z. Yang, P. Chen, Y. Hsieh, Y. Yao, M. Liao, M. Lee, M. Wang, and J. Hwang, Opt. Express **22**, A1589 (2014).
7. Z. Liu, T. Huang, J. Ma, C. Liu, and K. M. Lau, IEEE Electron Device Lett. **35**, 330 (2014).
8. Z. Liu, J. Ma, T. Huang, C. Liu, and K. M. Lau, Appl. Phys. Lett. **104**, 091103 (2014).
9. C. Liu, Z. Liu, T. Huang, J. Ma, and K. M. Lau, J. Cryst. Growth **414**, 243 (2015).
10. C. Liu, Y. Cai, Z. Liu, J. Ma, and K. M. Lau, Appl. Phys. Lett. **106**, 181110 (2015).
11. C. Liu, Y. Cai, H. Jiang, and K. M. Lau, J. Electron. Mater. **45**, 2092 (2016).
12. C. Liu, Y. Cai, X. Zou, and K. M. Lau, IEEE Photon. Technol. Lett. **28**, 1130 (2016).
13. Y.-F. Wu, B. P. Keller, S. Keller, D. Kapolnek, P. Kozodoy, S. P. Denbaars, and U. K. Mishra, Solid-State Electron. **41**, 1569 (1997).
14. Y. Cai, X. Zou, C. Liu, and K. M. Lau, IEEE Electron Device Lett. **39**, 224 (2018).